www.ietdl.org

Published in IET Signal Processing
Received on 17th August 2011
Revised on 18th January 2012
doi: 10.1049/iet-spr.2011.0313

Special Issue on Multi-Sensor Signal Processing for Defence: Detection, Localisation & Classification

ISSN 1751-9675

Generalised parametric Rao test for multi-channel adaptive detection of range-spread targets

P. Wang[1] *H. Li*[1] *T.R. Kavala*[1] *B. Himed*[2]

[1]*Department of Electrical and Computer Engineering, Stevens Institute of Technology, Hoboken, NJ 07030, USA*
[2]*AFRL/RYMD, 2241 Avionics Circle, Bldg 620, Dayton, OH 45433, USA*
E-mail: pwang4@stevens.edu

Abstract: This study considers the problem of detecting a multi-channel signal of range-spread targets in a homogeneous environment, where the disturbances in both test signal and training signals share the same covariance matrix. To this end, a generalised parametric Rao (GP-Rao) test is developed by modelling the disturbance as a multi-channel auto-regressive process. The GP-Rao test uses less training data and is computationally more efficient, when compared with conventional covariance matrix-based solutions. The theoretical detection performance of the GP-Rao test is characterised in terms of the asymptotic distribution under both hypotheses. Numerical results indicate that the proposed GP-Rao test attains asymptotically the constant false alarm rate property. Numerical results show that the GP-Rao test achieves better detection performance and uses significantly less training signals than the covariance matrix-based approach.

1 Introduction

It is well known that range resolution in radar is normally inversely proportional to the bandwidth of its transmitting pulses. Nowadays, wideband high-resolution radars can spatially resolve a target into a number of scattering centres depending on the range extent of the target and range resolution capabilities of the radar [1–5]. The high-resolution radar conveys abundant target information and has been successfully applied in target detection, localisation, classification and imaging. Range-spread target detection, which is very challenging in the high-resolution radar, has received considerable attention over the past decade [3–20]. It is shown to be statistically equivalent in detecting a target across a number of adjacent range cells in interferences with an unknown covariance matrix. In this paper, we consider the range-spread target detection problem in a high-resolution radar which employs multiple sensors and multiple pulses. With multiple sensors and pulses, the sensor array often uses space–time adaptive processing (STAP) for its enhanced target discrimination capability, compared with space- or time-only processing [21, 22].

Detection of range-spread targets in white Gaussian noise is addressed in [3], where some a priori statistical knowledge about the range-spread target is incorporated into the detection problem from a Bayesian framework. In [4], a modified generalised likelihood ratio test (MGLRT) is proposed for detecting range-spread targets embedded in correlated Gaussian noise. However, it appears that the statistical distribution of the MGLRT under the null hypothesis is dependent on the unknown covariance matrix and, as a result, does not achieve a constant false alarm rate (CFAR) property. An enhanced algorithm is proposed in [4] and is shown to limit the CFAR property in a bounded region. In [5], the range-spread target detection is addressed by proposing two new detectors from the generalised likelihood ratio test (GLRT) principle, using either a one-step or a two-step procedure. The resulting detectors, including the generalised adaptive matched filter (GAMF) and the GLRT, use homogeneous training signals to estimate the unknown disturbance covariance matrix. Both detectors ensure the CFAR property. Recent additions to the literature, by taking account into the subspace structure of the disturbance, interferences because of sidelobe (orthogonal) targets, and other uncertainties on the range-spread targets, can be found in [10–14, 16]. Meanwhile, the range-spread target detection problem in non-Gaussian disturbances has been fully addressed in [6–8, 15] and references therein. A challenging issue in non-Gaussian environments is the covariance matrix estimation which usually has no closed-form solution.

By exploiting the inherent structure of the disturbance covariance matrix, a parametric approach is shown to be essential in reducing the computational burden and also mitigating the requirement of training signals [9, 23–33]. In [9], the spatial-only disturbance component is modelled as a 'scalar' auto-regressive (AR) process, and parametric detectors have been proposed to handle the mono-pulse environment. In this paper, we extend the parametric AR modelling of the disturbance into both the spatial and temporal domains. Paralleling our parametric solutions to the point-target case [26, 27, 30, 31], we propose a 'multi-channel' AR process for the disturbance in the range-spread scenario, which in addition to the spatial correlation across multiple sensors, explicitly takes the temporal correlation

across multiple pulses into account. In order to find a simple and closed-form solution, we consider the Rao test which only requires the maximum likelihood (ML) estimates of the nuisance parameters under the null hypothesis. The proposed Rao test for the range-spread target detection is referred to as the generalised parametric Rao (GP-Rao) test. Instead of the joint spatial–temporal processing of the covariance matrix-based detectors, the GP-Rao test employs successively a temporal whitening followed by a spatial whitening. As verified by numerical results, the GP-Rao test is seen to outperform its covariance matrix-based counterparts, such as the GAMF and GLRT detectors.

The remainder of this paper is organised as follows. Section 2 describes the signal model and the problem statement. In Section 3, we first summarise the general principle of the Rao test and then develop the GP-Rao test step-by-step. Its detection performance is characterised by the asymptotic distribution of the GP-Rao test variable in both hypotheses. Numerical results are presented in Section 4 and concluding remarks are provided in Section 5.

2 Signal model

The problem of interest is to decide whether one of the following two hypotheses is true

$$\begin{aligned} H_0&: \quad \boldsymbol{x}_l(n) = \boldsymbol{d}_l(n) \\ H_1&: \quad \boldsymbol{x}_l(n) = \alpha_l \boldsymbol{s}(n) + \boldsymbol{d}_l(n) \\ l &= 0, 1, \ldots, L-1, \quad n = 0, 1, \ldots, N-1 \end{aligned}$$

where all vectors are of dimension $J \times 1$, J denotes the number of sensors or spatial channels, N is the number of temporal observations or pulses, and L is the number of range bins where the target spreads. Herein, $\boldsymbol{x}_l(n)$ is referred to as the nth array snapshot of the test signal at the lth range bin, $\boldsymbol{s}(n)$ is the assumed known steering vector at the nth array snapshot, α_l is the unknown complex target amplitude at the lth range bin, and $\boldsymbol{d}_l(n)$ is the disturbance that is correlated in both space and time domains. Besides the test signals $\boldsymbol{x}_l(n)$, there are KL target-free training signals $\boldsymbol{x}_k(n)$ available

$$\boldsymbol{x}_k(n) = \boldsymbol{d}_k(n), \quad k = L, \ldots, (K+1)L-1 \tag{1}$$

Define the following $JN \times 1$ space–time vectors

$$\begin{aligned} \boldsymbol{s} &= [\boldsymbol{s}^{\mathrm{T}}(0), \boldsymbol{s}^{\mathrm{T}}(1), \ldots, \boldsymbol{s}^{\mathrm{T}}(N-1)]^{\mathrm{T}} \\ \boldsymbol{d}_k &= [\boldsymbol{d}_k^{\mathrm{T}}(0), \boldsymbol{d}_k^{\mathrm{T}}(1), \ldots, \boldsymbol{d}_k^{\mathrm{T}}(N-1)]^{\mathrm{T}} \\ \boldsymbol{x}_k &= [\boldsymbol{x}_k^{\mathrm{T}}(0), \boldsymbol{x}_k^{\mathrm{T}}(1), \ldots, \boldsymbol{x}_k^{\mathrm{T}}(N-1)]^{\mathrm{T}} \end{aligned}$$

where $k = 0, 1, \ldots, (K+1)L-1$. The problem of interest can be equivalently described as the following binary composite hypothesis testing problem

$$\begin{aligned} H_0&: \quad \boldsymbol{x}_l = \boldsymbol{d}_l, \quad \boldsymbol{x}_k = \boldsymbol{d}_k \\ H_1&: \quad \boldsymbol{x}_l = \alpha_l \boldsymbol{s} + \boldsymbol{d}_l, \quad \boldsymbol{x}_k = \boldsymbol{d}_k \\ l &= 0, 1, \ldots, L-1 \\ k &= L, \ldots, (K+1)L-1 \end{aligned}$$

A common assumption in the literature [3–5] is that: disturbances $\{\boldsymbol{d}_l\}_{l=0}^{L-1}$ in the test signals and those in the training signals $\{\boldsymbol{d}_k\}_{k=L}^{(K+1)L-1}$ are assumed to be mutually independent with the same statistical distribution $\mathcal{CN}(\boldsymbol{0}, \boldsymbol{R})$, where $\boldsymbol{R}$ is the unknown space–time covariance matrix. In this paper, a multi-channel AR process is employed to model the space–time disturbance and we have the following parametric modelling for the disturbances [23, 26, 27, 30, 31]:

- AS1: The disturbances $\boldsymbol{d}_k(n)$, $k = 0, \ldots, (K+1)L-1$, in both the test and training signals can be modelled as a J-channel AR(P) process with model order P:

$$\boldsymbol{d}_k(n) = -\sum_{i=1}^{P} \boldsymbol{A}^{\mathrm{H}}(i) \boldsymbol{d}_k(n-i) + \boldsymbol{\varepsilon}_k(n) \tag{2}$$

where $\{\boldsymbol{A}^{\mathrm{H}}(i)\}_{i=1}^{P}$ denote the 'unknown' $J \times J$ AR coefficient matrices, $\boldsymbol{\varepsilon}_k(n)$ denote the $J \times 1$ spatial noise vectors that are temporally white but spatially coloured: $\boldsymbol{\varepsilon}_k(n) \sim \mathcal{CN}(\boldsymbol{0}, \boldsymbol{Q})$ and $\boldsymbol{Q}$ denotes the 'unknown' $J \times J$ spatial covariance matrix.

The problem of interest is finally to develop a decision rule for the above composite hypothesis testing problem based on the signal model and the assumption AS1.

3 GP-Rao test for range-spread target detection

In fact, the above problem of interest is a composite hypothesis test, which means that there is no a uniformly most powerful (UMP) test for the problem. Suboptimum alternatives such as the GLRT is commonly adopted in practice and works well in many circumstances [34]. Nevertheless, the GLRT for the above range-spread target detection in the AR modelled disturbance has no exactly closed-form solution [27, 30]. Therefore we resort to the Rao test, a simpler solution than the GLRT, which only requires the ML estimates of the nuisance parameters under H_0. Moreover, the Rao test has been verified that it achieves the CFAR property and may perform as well as the GLRT asymptotically [26, 34, 35].

In general, the Rao test is computed as [34]

$$T_{\mathrm{Rao}} = \frac{\partial \ln f(\boldsymbol{\theta})}{\partial \boldsymbol{\theta}_r}\bigg|_{\boldsymbol{\theta}=\tilde{\boldsymbol{\theta}}}^{\mathrm{T}} [\boldsymbol{I}^{-1}(\tilde{\boldsymbol{\theta}})]_{\boldsymbol{\theta}_r, \boldsymbol{\theta}_r} \frac{\partial \ln f(\boldsymbol{\theta})}{\partial \boldsymbol{\theta}_r}\bigg|_{\boldsymbol{\theta}=\tilde{\boldsymbol{\theta}}} \tag{3}$$

where according to the signal model of Section 2,

- $f(\boldsymbol{\theta})$ denotes the joint probability density function (pdf) of the test and training signals.
- $\boldsymbol{\theta}_r = [\boldsymbol{\alpha}_{\mathrm{R}}^{\mathrm{T}}, \boldsymbol{\alpha}_{\mathrm{I}}^{\mathrm{T}}]^{\mathrm{T}} = [\Re\{\boldsymbol{\alpha}^{\mathrm{T}}\}, \Im\{\boldsymbol{\alpha}^{\mathrm{T}}\}]^{\mathrm{T}}$ denotes the $2L \times 1$ 'signal parameter' vector, where $\Re$ and $\Im$ denote the real and imaginary parts, respectively, and $\boldsymbol{\alpha} = [\alpha_1, \alpha_2, \ldots, \alpha_L]$ stacks the L target amplitudes into an $L \times 1$ complex vector. The joint pdf under H_0 and the pdf under H_1 differ only in the value of θ_r, where $\boldsymbol{\theta}_{r_0} = \boldsymbol{0}_{2L \times 1}$ and $\boldsymbol{\theta}_{r_1} = [\boldsymbol{\alpha}_{\mathrm{R}}^{\mathrm{T}}, \boldsymbol{\alpha}_{\mathrm{I}}^{\mathrm{T}}]^{\mathrm{T}}$;
- $\boldsymbol{\theta}_s = [\boldsymbol{q}_{\mathrm{R}}^{\mathrm{T}}, \boldsymbol{q}_{\mathrm{I}}^{\mathrm{T}}, \boldsymbol{a}_{\mathrm{R}}^{\mathrm{T}}, \boldsymbol{a}_{\mathrm{I}}^{\mathrm{T}}]^{\mathrm{T}}$ denotes the 'nuisance parameter' vector with $\boldsymbol{a}_{\mathrm{R}}^{\mathrm{T}} = \mathrm{vec}(\Re\{\boldsymbol{A}^{\mathrm{H}}\})$, $\boldsymbol{a}_{\mathrm{I}}^{\mathrm{T}} = \mathrm{vec}(\Im\{\boldsymbol{A}^{\mathrm{H}}\})$, $\boldsymbol{q}_{\mathrm{R}}^{\mathrm{T}}$ contains the diagonal elements in $\boldsymbol{Q}$ and the real part of the elements below the diagonal, whereas $\boldsymbol{q}_{\mathrm{I}}^{\mathrm{T}}$ contains the imaginary part of the elements below the diagonal;
- $\boldsymbol{\theta} = [\boldsymbol{\theta}_r^{\mathrm{T}}, \boldsymbol{\theta}_s^{\mathrm{T}}]^{\mathrm{T}}$ contains all unknown parameters;
- $\tilde{\boldsymbol{\theta}} = [\boldsymbol{\theta}_{r_0}^{\mathrm{T}}, \hat{\boldsymbol{\theta}}_{s_0}^{\mathrm{T}}]^{\mathrm{T}}$ denotes the ML estimate of $\boldsymbol{\theta}$ under H_0.
- $\boldsymbol{I}^{-1}(\boldsymbol{\theta})$ is the inverse of the Fisher information matrix (FIM) at the estimate of $\boldsymbol{\theta}$ under H_0, and the FIM is

partitioned as [34]

$$\boldsymbol{I}(\boldsymbol{\theta}) = \begin{bmatrix} \boldsymbol{I}_{\boldsymbol{\theta}_r,\boldsymbol{\theta}_r}(\boldsymbol{\theta}) & \boldsymbol{I}_{\boldsymbol{\theta}_r,\boldsymbol{\theta}_s}(\boldsymbol{\theta}) \\ \boldsymbol{I}_{\boldsymbol{\theta}_s,\boldsymbol{\theta}_r}(\boldsymbol{\theta}) & \boldsymbol{I}_{\boldsymbol{\theta}_s,\boldsymbol{\theta}_s}(\boldsymbol{\theta}) \end{bmatrix} \tag{4}$$

• $[\boldsymbol{I}^{-1}(\tilde{\boldsymbol{\theta}})]_{\boldsymbol{\theta}_r,\boldsymbol{\theta}_r}$ denotes the subblock matrix of the inverse FIM corresponding to the signal parameter $\boldsymbol{\theta}_r$ under H_0, which is computed as

$$[\boldsymbol{I}^{-1}(\tilde{\boldsymbol{\theta}})]_{\boldsymbol{\theta}_r,\boldsymbol{\theta}_r} = (\boldsymbol{I}_{\boldsymbol{\theta}_r,\boldsymbol{\theta}_r}(\tilde{\boldsymbol{\theta}}) - \boldsymbol{I}_{\boldsymbol{\theta}_r,\boldsymbol{\theta}_s}(\tilde{\boldsymbol{\theta}})\boldsymbol{I}^{-1}_{\boldsymbol{\theta}_s,\boldsymbol{\theta}_s}(\tilde{\boldsymbol{\theta}})\boldsymbol{I}_{\boldsymbol{\theta}_s,\boldsymbol{\theta}_r}(\tilde{\boldsymbol{\theta}}))^{-1} \tag{5}$$

where we invoke the inverse of the FIM block matrix in (4).

As a result, the development of the GP-Rao test requires the ML estimates of the nuisance parameters $\boldsymbol{\theta}_s$, that is, $\hat{\boldsymbol{\theta}}_{s_0}$, under the null hypothesis and the FIM-related term $[\boldsymbol{I}^{-1}(\tilde{\boldsymbol{\theta}})]_{\boldsymbol{\theta}_r,\boldsymbol{\theta}_r}$ corresponding to the signal parameter $\boldsymbol{\theta}_r$, which will be sequentially addressed in the following two subsections.

3.1 ML estimation under the null hypothesis

In the following, we derive the ML estimates of the nuisance parameters $\boldsymbol{Q}$ and $\boldsymbol{A} = [\boldsymbol{A}(1)^{\mathrm{T}}, \boldsymbol{A}(2)^{\mathrm{T}}, \ldots, \boldsymbol{A}(P)^{\mathrm{T}}]^{\mathrm{T}}$ under H_0. Since the test signals and the training signals are independent, the joint pdf $f_i(\boldsymbol{X}|\alpha, \boldsymbol{A}, \boldsymbol{Q})$ ($f_i(\boldsymbol{X}|\boldsymbol{\theta})$ for short), conditioned on the first P elements, can be expressed as

$$f_i(\boldsymbol{X}|\boldsymbol{\alpha}, \boldsymbol{A}, \boldsymbol{Q}) = \left[\frac{1}{\pi^J|\boldsymbol{Q}|}\mathrm{e}^{-\mathrm{tr}\{\boldsymbol{Q}^{-1}\boldsymbol{T}_i(\boldsymbol{\alpha},\boldsymbol{A})\}}\right]^{L(K+1)(N-P)} \tag{6}$$

where

$$\begin{aligned} &L(K+1)(N-P)\boldsymbol{T}_i(\boldsymbol{\alpha}, \boldsymbol{A}) \\ &= \sum_{l=0}^{L-1}\sum_{n=P}^{N-1}\boldsymbol{\varepsilon}_l(n)\boldsymbol{\varepsilon}_l^{\mathrm{H}}(n) + \sum_{k=L}^{(K+1)L-1}\sum_{n=P}^{N-1}\boldsymbol{\varepsilon}_k(n)\boldsymbol{\varepsilon}_k^{\mathrm{H}}(n) \end{aligned} \tag{7}$$

with $\boldsymbol{\varepsilon}_l(n)$, $l = 0, 1, \ldots, L-1$, denoting the 'temporally whitened target-free' test signals

$$\begin{aligned} \boldsymbol{\varepsilon}_l(n) &= \tilde{\boldsymbol{x}}_l(n) - \alpha_l\tilde{\boldsymbol{s}}(n) \\ &= \left[\boldsymbol{x}_l(n) + \sum_{p=1}^{P}\boldsymbol{A}^{\mathrm{H}}(p)\boldsymbol{x}_l(n-p)\right] \\ &\quad - \alpha_l\left[\boldsymbol{s}(n) + \sum_{p=1}^{P}\boldsymbol{A}^{\mathrm{H}}(p)\boldsymbol{s}(n-p)\right] \end{aligned} \tag{8}$$

and, respectively, $\boldsymbol{\varepsilon}_k(n)$, $k = L, L+1, \ldots, (K+1)L-1$, denoting the 'temporally whitened' training signals

$$\boldsymbol{\varepsilon}_k(n) = \boldsymbol{x}_k(n) + \sum_{p=1}^{P}\boldsymbol{A}^{\mathrm{H}}(p)\boldsymbol{x}_k(n-p) \tag{9}$$

Note here that $\boldsymbol{\alpha} \neq \boldsymbol{0}$ under H_1 (i.e. $i = 1$), and $\boldsymbol{\alpha} = \boldsymbol{0}$ under H_0 (i.e. $i = 0$), which results in the joint pdf $f_0(\boldsymbol{X}|\boldsymbol{\theta})$ under H_0 [as well as $\boldsymbol{T}_0$ and $\boldsymbol{\varepsilon}_l(n)$] being independent of the signal parameter $\boldsymbol{\alpha}$.

By setting $\boldsymbol{\alpha} = 0$ in (6), taking the derivative of the log-likelihood, that is, $\ln f_0(\boldsymbol{X}|\boldsymbol{A}, \boldsymbol{Q})$, with respect to (w.r.t.) $\boldsymbol{Q}$, and equating it to zero, we obtain the ML estimate of $\boldsymbol{Q}$ as

$$\hat{\boldsymbol{Q}}_{\mathrm{ML}}(\boldsymbol{A}) = \boldsymbol{T}_0(\boldsymbol{A}) \tag{10}$$

where $\boldsymbol{T}_0(\boldsymbol{A})$ is defined in (7) by setting $\boldsymbol{\alpha} = 0$.

Substituting $\hat{\boldsymbol{Q}}_{\mathrm{ML}}(\boldsymbol{A})$ into the log-likelihood function $\ln f(\boldsymbol{X}|\boldsymbol{A}, \boldsymbol{Q})$ yields

$$f_0(\boldsymbol{X}|\boldsymbol{A}, \hat{\boldsymbol{Q}}_{\mathrm{ML}}) = \left[\frac{(\mathrm{e}\pi)^{-J}}{|\boldsymbol{T}_0(\boldsymbol{A})|}\right]^{L(K+1)(N-P)} \tag{11}$$

It is seen that maximising $f_0(\boldsymbol{X}|\boldsymbol{A}, \hat{\boldsymbol{Q}}_{\mathrm{ML}})$ w.r.t. $\boldsymbol{A}$ is equivalent to minimising $|\boldsymbol{T}_0(\boldsymbol{A})|$. Note that

$$\begin{aligned} &L(K+1)(N-P)\boldsymbol{T}_0(\boldsymbol{A}) \\ &= \sum_{l=0}^{L-1}\sum_{n=P}^{N-1}\boldsymbol{\varepsilon}_l(n)\boldsymbol{\varepsilon}_l^{\mathrm{H}}(n) + \sum_{k=L}^{(K+1)L-1}\sum_{n=P}^{N-1}\boldsymbol{\varepsilon}_k(n)\boldsymbol{\varepsilon}_k^{\mathrm{H}}(n) \\ &= \hat{\boldsymbol{R}}_{xx} + \boldsymbol{A}^{\mathrm{H}}\hat{\boldsymbol{R}}_{yx} + \hat{\boldsymbol{R}}_{yx}^{\mathrm{H}}\boldsymbol{A} + \boldsymbol{A}^{\mathrm{H}}\hat{\boldsymbol{R}}_{yy}\boldsymbol{A} \\ &= (\boldsymbol{A}^{\mathrm{H}} + \hat{\boldsymbol{R}}_{yx}^{\mathrm{H}}\hat{\boldsymbol{R}}_{yy}^{-1})\hat{\boldsymbol{R}}_{yy}(\boldsymbol{A}^{\mathrm{H}} + \hat{\boldsymbol{R}}_{yx}^{\mathrm{H}}\hat{\boldsymbol{R}}_{yy}^{-1})^{\mathrm{H}} \\ &\quad + \hat{\boldsymbol{R}}_{xx} - \hat{\boldsymbol{R}}_{yx}^{\mathrm{H}}\hat{\boldsymbol{R}}_{yy}^{-1}\hat{\boldsymbol{R}}_{yx} \end{aligned} \tag{12}$$

where

$$\hat{\boldsymbol{R}}_{xx} = \sum_{l=0}^{L-1}\sum_{n=P}^{N-1}\boldsymbol{x}_l(n)\boldsymbol{x}_l^{\mathrm{H}}(n) + \sum_{k=L}^{L(K+1)-1}\sum_{n=P}^{N-1}\boldsymbol{x}_k(n)\boldsymbol{x}_k^{\mathrm{H}}(n) \tag{13}$$

$$\hat{\boldsymbol{R}}_{yy} = \sum_{l=0}^{L-1}\sum_{n=P}^{N-1}\boldsymbol{y}_l(n)\boldsymbol{y}_l^{\mathrm{H}}(n) + \sum_{k=L}^{L(K+1)-1}\sum_{n=P}^{N-1}\boldsymbol{y}_k(n)\boldsymbol{y}_k^{\mathrm{H}}(n) \tag{14}$$

$$\hat{\boldsymbol{R}}_{yx} = \sum_{l=0}^{L-1}\sum_{n=P}^{N-1}\boldsymbol{y}_l(n)\boldsymbol{x}_l^{\mathrm{H}}(n) + \sum_{k=L}^{L(K+1)-1}\sum_{n=P}^{N-1}\boldsymbol{y}_k(n)\boldsymbol{x}_k^{\mathrm{H}}(n) \tag{15}$$

with two regressive vectors of the test signals and the training signals defined, respectively, as follows

$$\begin{aligned} &\boldsymbol{y}_l(n) = [\boldsymbol{x}_l^{\mathrm{T}}(n-1), \boldsymbol{x}_l^{\mathrm{T}}(n-2), \ldots, \boldsymbol{x}_l^{\mathrm{T}}(n-P)]^{\mathrm{T}} \\ &\quad l = 0, 1, \ldots, L-1 \end{aligned} \tag{16}$$

$$\begin{aligned} &\boldsymbol{y}_k(n) = [\boldsymbol{x}_k^{\mathrm{T}}(n-1), \boldsymbol{x}_k^{\mathrm{T}}(n-2), \ldots, \boldsymbol{x}_k^{\mathrm{T}}(n-P)]^{\mathrm{T}} \\ &\quad k = L, L+1, \ldots, (K+1)L-1 \end{aligned} \tag{17}$$

From (12), since $\hat{\boldsymbol{R}}_{yy}$ is non-negative definite and the remaining terms in (12) do not depend on $\boldsymbol{A}$, it follows that

$$\begin{aligned} &L(K+1)(N-P)\boldsymbol{T}_0(\boldsymbol{A}) \geq L(K+1)(N-P)\boldsymbol{T}_0(\hat{\boldsymbol{A}}_{\mathrm{ML}}) \\ &\quad = \hat{\boldsymbol{R}}_{xx} - \hat{\boldsymbol{R}}_{yx}^{\mathrm{H}}\hat{\boldsymbol{R}}_{yy}^{-1}\hat{\boldsymbol{R}}_{yx} \end{aligned} \tag{18}$$

where

$$\hat{\boldsymbol{A}}_{\mathrm{ML}} = -\hat{\boldsymbol{R}}_{yy}^{-1}\hat{\boldsymbol{R}}_{yx} \tag{19}$$

with $\hat{\boldsymbol{R}}_{yy}$ and $\hat{\boldsymbol{R}}_{yx}$ defined in (14) and (15). Once $\boldsymbol{T}_0(\boldsymbol{A})$ is minimised, $\hat{\boldsymbol{A}}_{\mathrm{ML}}$ will minimise any non-decreasing function including the determinant of $\boldsymbol{T}_0(\boldsymbol{A})$.

In summary, the ML estimate of $\boldsymbol{A}$ is obtained in (19) and the ML estimate of $\boldsymbol{Q}$ is obtained in (10) by replacing

doi: 10.1049/iet-spr.2011.0313

$\boldsymbol{A}$ with $\hat{\boldsymbol{A}}_{\mathrm{ML}}$, that is

$$\hat{\boldsymbol{Q}}_{\mathrm{ML}} = \boldsymbol{T}_0(\hat{\boldsymbol{A}}_{\mathrm{ML}}) = \frac{\hat{\boldsymbol{R}}_{xx} - \hat{\boldsymbol{R}}_{yx}^{\mathrm{H}}\hat{\boldsymbol{R}}_{yy}^{-1}\hat{\boldsymbol{R}}_{yx}}{L(K+1)(N-P)} \tag{20}$$

where the second equality is due to (18).

3.2 Fisher information matrix

The second step to derive the GP-Rao test is to obtain the FIM-related term $[\boldsymbol{I}^{-1}(\tilde{\boldsymbol{\theta}})]_{\boldsymbol{\theta}_r,\boldsymbol{\theta}_r}$, which requires to evaluate the first-order and second-order derivatives of the log-likelihood function $\ln f_1(\boldsymbol{X}|\boldsymbol{\alpha}, \boldsymbol{A}, \boldsymbol{Q})$ w.r.t. all unknown parameters.

First, it is seen that the mean of the (Gaussian) measurements is related to the signal parameter $\boldsymbol{\theta}_r = \boldsymbol{\alpha}$, whereas the covariance matrix of the measurements is a function of $\boldsymbol{A}$ and $\boldsymbol{Q}$ (or, equivalently, $\boldsymbol{\theta}_s$). Since the mean and the covariance matrix are decoupled (they do not share common parameters), the FIM of the estimates of all unknown parameter $\boldsymbol{\theta}$ is block diagonal; see [34, Section 3.9]. In other words, we have

$$\boldsymbol{I}_{\boldsymbol{\theta}_r,\boldsymbol{\theta}_s}(\boldsymbol{\theta}) = \boldsymbol{0}, \quad \boldsymbol{I}_{\boldsymbol{\theta}_s,\boldsymbol{\theta}_r}(\boldsymbol{\theta}) = \boldsymbol{0} \tag{21}$$

By substituting the above results into (5), we simplify the term $[\boldsymbol{I}^{-1}(\tilde{\boldsymbol{\theta}})]_{\boldsymbol{\theta}_r,\boldsymbol{\theta}_r}$ in the Rao test as

$$[\boldsymbol{I}^{-1}(\tilde{\boldsymbol{\theta}})]_{\boldsymbol{\theta}_r,\boldsymbol{\theta}_r} = \boldsymbol{I}^{-1}_{\boldsymbol{\theta}_r,\boldsymbol{\theta}_r}(\tilde{\boldsymbol{\theta}}) \tag{22}$$

Therefore in the following, we concentrate on calculating the block matrix of the FIM corresponding to the signal parameters $\boldsymbol{\theta}_r$.

The first partial derivatives of the log-likelihood function $\ln f_1(\boldsymbol{X}|\boldsymbol{\theta})$ w.r.t. the $2L \times 1$ signal parameters $\boldsymbol{\theta}_r = [\boldsymbol{\alpha}_{\mathrm{R}}^{\mathrm{T}}, \boldsymbol{\alpha}_{\mathrm{I}}^{\mathrm{T}}]^{\mathrm{T}}$ are

$$\frac{\partial \ln f_1(\boldsymbol{X}|\boldsymbol{\theta})}{\partial \boldsymbol{\theta}_r} = \begin{bmatrix} \dfrac{\partial \ln f_1(\boldsymbol{X}|\boldsymbol{\theta})}{\partial \boldsymbol{\alpha}_{\mathrm{R}}} \\ \dfrac{\partial \ln f_1(\boldsymbol{X}|\boldsymbol{\theta})}{\partial \boldsymbol{\alpha}_{\mathrm{I}}} \end{bmatrix} \tag{23}$$

where we use the joint pdf of (6) and invoke the independence across the test signal

$$\left[\frac{\partial \ln f_1(\boldsymbol{X}|\boldsymbol{\theta})}{\partial \boldsymbol{\alpha}_{\mathrm{R}}}\right]_l = \sum_{n=P}^{N-1} [\tilde{\boldsymbol{s}}^{\mathrm{H}}(n)\boldsymbol{Q}^{-1}\boldsymbol{\varepsilon}_l(n) + \boldsymbol{\varepsilon}_l^{\mathrm{H}}(n)\boldsymbol{Q}^{-1}\tilde{\boldsymbol{s}}(n)] \tag{24}$$

$$\left[\frac{\partial \ln f_1(\boldsymbol{X}|\boldsymbol{\theta})}{\partial \boldsymbol{\alpha}_{\mathrm{I}}}\right]_l = \mathrm{j}\sum_{n=P}^{N-1} [\tilde{\boldsymbol{s}}^{\mathrm{H}}(n)\boldsymbol{Q}^{-1}\boldsymbol{\varepsilon}_l(n) - \boldsymbol{\varepsilon}_l^{\mathrm{H}}(n)\boldsymbol{Q}^{-1}\tilde{\boldsymbol{s}}(n)] \tag{25}$$

where $\tilde{\boldsymbol{s}}(n)$ is the temporally whitened steering vector defined in (8) and $\boldsymbol{\varepsilon}_l$ is the temporally whitened test signal at the lth range bin which is also defined in (8).

The second partial derivatives of $\ln f_1(\boldsymbol{X}|\boldsymbol{\theta})$ w.r.t. $\boldsymbol{\theta}_r$ are shown below

$$\frac{\partial^2 \ln f_1(\boldsymbol{X}|\boldsymbol{\theta})}{\partial\{\boldsymbol{\alpha}_{\mathrm{R}}\}_l \partial\{\boldsymbol{\alpha}_{\mathrm{R}}\}_\ell} = -2\delta(l-\ell)\sum_{n=P}^{N-1} \tilde{\boldsymbol{s}}^{\mathrm{H}}(n)\boldsymbol{Q}^{-1}\tilde{\boldsymbol{s}}(n)$$

$$\frac{\partial^2 \ln f_1(\boldsymbol{X}|\boldsymbol{\theta})}{\partial\{\boldsymbol{\alpha}_{\mathrm{I}}\}_l \partial\{\boldsymbol{\alpha}_{\mathrm{I}}\}_\ell} = -2\delta(l-\ell)\sum_{n=P}^{N-1} \tilde{\boldsymbol{s}}^{\mathrm{H}}(n)\boldsymbol{Q}^{-1}\tilde{\boldsymbol{s}}(n)$$

$$\frac{\partial^2 \ln f_1(\boldsymbol{X}|\boldsymbol{\theta})}{\partial\{\boldsymbol{\alpha}_{\mathrm{R}}\}_l \partial\{\boldsymbol{\alpha}_I\}_\ell} = \frac{\partial^2 \ln f_1(\boldsymbol{X}|\boldsymbol{\theta})}{\partial\{\boldsymbol{\alpha}_I\}_l \partial\{\boldsymbol{\alpha}_{\mathrm{R}}\}_\ell} = 0$$

where $\{\boldsymbol{v}_l\}$ denotes the lth element of the vector $\boldsymbol{v}$, and $\boldsymbol{\delta}(l)$ is the Kronecker delta function. Substituting the above elements back into $\boldsymbol{I}_{\boldsymbol{\theta}_r,\boldsymbol{\theta}_r}(\boldsymbol{\theta})$, we have

$$[\boldsymbol{I}(\boldsymbol{\theta})]_{\boldsymbol{\theta}_r,\boldsymbol{\theta}_r} = 2\sum_{n=P}^{N-1} \tilde{\boldsymbol{s}}^{\mathrm{H}}(n)\boldsymbol{Q}^{-1}\tilde{\boldsymbol{s}}(n)\boldsymbol{I}_{2L} \tag{26}$$

where $\boldsymbol{I}_{2L}$ denotes the identity matrix with a dimension of $2L$. According to (22), the FIM-related term $[\boldsymbol{I}^{-1}(\tilde{\boldsymbol{\theta}})]_{\boldsymbol{\theta}_r,\boldsymbol{\theta}_r}$ is obtained as

$$\begin{aligned}[\boldsymbol{I}^{-1}(\tilde{\boldsymbol{\theta}})]_{\boldsymbol{\theta}_r,\boldsymbol{\theta}_r} &= \boldsymbol{I}^{-1}_{\boldsymbol{\theta}_r,\boldsymbol{\theta}_r}(\tilde{\boldsymbol{\theta}}) = \boldsymbol{I}^{-1}_{\boldsymbol{\theta}_r,\boldsymbol{\theta}_r}(\boldsymbol{\theta})|_{\boldsymbol{\theta}=\tilde{\boldsymbol{\theta}}} \\ &= \frac{1}{2\sum_{n=P}^{N-1} \hat{\tilde{\boldsymbol{s}}}^{\mathrm{H}}(n)\hat{\boldsymbol{Q}}_{\mathrm{ML}}^{-1}\hat{\tilde{\boldsymbol{s}}}(n)}\boldsymbol{I}_{2L}\end{aligned} \tag{27}$$

where $\hat{\boldsymbol{Q}}_{\mathrm{ML}}$, as given by (20), is the ML estimate of $\boldsymbol{Q}$ under H_0, and the temporally whitened steering vector $\hat{\tilde{\boldsymbol{s}}}$ is given by

$$\hat{\tilde{\boldsymbol{s}}}(n) = \boldsymbol{s}(n) + \sum_{p=1}^{P} \hat{\boldsymbol{A}}_{\mathrm{ML}}^{\mathrm{H}}(p)\boldsymbol{s}(n-p) \tag{28}$$

with $\hat{\boldsymbol{A}}_{\mathrm{ML}}$ given by (19).

3.3 GP-Rao test

From (8), we obtain

$$\varepsilon_l(n)|_{\boldsymbol{\theta}=\tilde{\boldsymbol{\theta}}} = \hat{\tilde{\boldsymbol{x}}}_l(n) = \boldsymbol{x}_l(n) + \sum_{p=1}^{P} \hat{\boldsymbol{A}}_{\mathrm{ML}}^{\mathrm{H}}(p)\boldsymbol{x}_l(n-p) \tag{29}$$

Then, based on (24) and (25), the first-order derivatives of the log-likelihood function at $\boldsymbol{\theta} = \tilde{\boldsymbol{\theta}}$ are simplified to

$$\left[\frac{\partial \ln f_1(\boldsymbol{X}|\tilde{\boldsymbol{\theta}})}{\partial \boldsymbol{\alpha}_{\mathrm{R}}}\right]_l = \sum_{n=P}^{N-1} [\hat{\tilde{\boldsymbol{s}}}^{\mathrm{H}}(n)\hat{\boldsymbol{Q}}_{\mathrm{ML}}^{-1}\hat{\tilde{\boldsymbol{x}}}_l(n) + \hat{\tilde{\boldsymbol{x}}}_l^{\mathrm{H}}(n)\hat{\boldsymbol{Q}}_{\mathrm{ML}}^{-1}\hat{\tilde{\boldsymbol{s}}}(n)] \tag{30}$$

$$\left[\frac{\partial \ln f_1(\boldsymbol{X}|\tilde{\boldsymbol{\theta}})}{\partial \boldsymbol{\alpha}_{\mathrm{I}}}\right]_l = \mathrm{j}\sum_{n=P}^{N-1} [\hat{\tilde{\boldsymbol{s}}}^{\mathrm{H}}(n)\hat{\boldsymbol{Q}}_{\mathrm{ML}}^{-1}\hat{\tilde{\boldsymbol{x}}}_l(n) - \hat{\tilde{\boldsymbol{x}}}_l^{\mathrm{H}}(n)\hat{\boldsymbol{Q}}_{\mathrm{ML}}^{-1}\hat{\tilde{\boldsymbol{s}}}(n)] \tag{31}$$

In addition to the ML estimates of nuisance parameters under H_0 and the FIM-related item, the general Rao test of (3)

reduces to the GP-Rao test

$$T_{\text{GP-Rao}} = \frac{2\sum_{l=0}^{L-1}\left|\sum_{n=P}^{N-1}\hat{\tilde{\boldsymbol{s}}}^{\text{H}}(n)\hat{\boldsymbol{Q}}_{\text{ML}}^{-1}\hat{\tilde{\boldsymbol{x}}}_l(n)\right|^2}{\sum_{n=P}^{N-1}\hat{\tilde{\boldsymbol{s}}}^{\text{H}}(n)\hat{\boldsymbol{Q}}_{\text{ML}}^{-1}\hat{\tilde{\boldsymbol{s}}}(n)} \underset{H_0}{\overset{H_1}{\gtrless}} \gamma_{\text{GP-Rao}} \quad (32)$$

where $\gamma_{\text{GP-Rao}}$ is the threshold subject to a given probability of false alarm, $\hat{\boldsymbol{Q}}_{\text{ML}}$ denotes the ML estimate of the spatial covariance matrix; see (20), and $\hat{\tilde{\boldsymbol{s}}}(n)$ and $\hat{\tilde{\boldsymbol{x}}}_l(n)$ are, respectively, the 'temporally whitened' steering vector and the lth test signal by using the ML estimates of $\boldsymbol{A}$; see (28) and (29).

From (32), it is seen that the GP-Rao test preforms successively a temporal whitening followed by a spatial whitening. Particularly, the steering vector $\boldsymbol{s}(n)$ and the lth test signal $\boldsymbol{x}_l(n)$ are temporally whitened according to (28) and (29) with the ML estimate $\hat{\boldsymbol{A}}_{\text{ML}}$, whereas the spatial whitening is performed by using the ML estimate $\hat{\boldsymbol{Q}}_{\text{ML}}$. It is also noted that the temporal and spatial whitening use both the test signals and training signal through the ML estimates $\hat{\boldsymbol{A}}_{\text{ML}}$ of (19) and $\hat{\boldsymbol{Q}}_{\text{ML}}$ of (20).

The proposed GP-Rao test can also be connected to the conventional parametric Rao test for the point-target detection [26]. Rewrite the GP-Rao test variable as

$$\begin{aligned} T_{\text{GP-Rao}} &= \sum_{l=0}^{L-1}\frac{2\left|\sum_{n=P}^{N-1}\hat{\tilde{\boldsymbol{s}}}^{\text{H}}(n)\hat{\boldsymbol{Q}}_{\text{ML}}^{-1}\hat{\tilde{\boldsymbol{x}}}_l(n)\right|^2}{\sum_{n=P}^{N-1}\hat{\tilde{\boldsymbol{s}}}^{\text{H}}(n)\hat{\boldsymbol{Q}}_{\text{ML}}^{-1}\hat{\tilde{\boldsymbol{s}}}(n)} \\ &= \sum_{l=0}^{L-1} T_{\text{GP-Rao}}(l) \end{aligned} \quad (33)$$

where $T_{\text{GP-Rao}}(l)$ denotes the local GP-Rao test statistic for the lth test signal. It is seen that the local GP-Rao test $T_{\text{GP-Rao}}(l)$ shares the 'same' detection variable of the conventional parametric Rao test $T_{\text{P-Rao}}(l)$ for the lth range bin (see [26, eq. (18)]) but with 'different' ML estimates of unknown parameters $\boldsymbol{A}$ and $\boldsymbol{Q}$. More specifically, the conventional parametric Rao test $T_{\text{P-Rao}}(l)$ for the lth test signal is given by

$$T_{\text{P-Rao}}(l) = \frac{2\left|\sum_{n=P}^{N-1}\hat{\tilde{\boldsymbol{s}}}_{\text{LML}}^{\text{H}}(n)\hat{\boldsymbol{Q}}_{\text{LML}}^{-1}\hat{\tilde{\boldsymbol{x}}}_{\text{LML},l}(n)\right|^2}{\sum_{n=P}^{N-1}\hat{\tilde{\boldsymbol{s}}}_{\text{LML}}^{\text{H}}(n)\hat{\boldsymbol{Q}}_{\text{LML}}^{-1}\hat{\tilde{\boldsymbol{s}}}_{\text{LML}}(n)} \quad (34)$$

where $\hat{\boldsymbol{A}}_{\text{LML}}$ and $\hat{\boldsymbol{Q}}_{\text{LML}}$ are the local ML estimates [26, eqs. (23)–(25)]

$$\hat{\boldsymbol{A}}_{\text{LML}} = -\hat{\boldsymbol{R}}_{yy,l}^{-1}\hat{\boldsymbol{R}}_{yx,l} \quad (35)$$

$$\hat{\boldsymbol{Q}}_{\text{LML}} = \frac{\hat{\boldsymbol{R}}_{xx,l} - \hat{\boldsymbol{R}}_{yx,l}^{\text{H}}\hat{\boldsymbol{R}}_{yy,l}^{-1}\hat{\boldsymbol{R}}_{yx,l}}{(KL+1)(N-P)} \quad (36)$$

with

$$\hat{\boldsymbol{R}}_{xx,l} = \sum_{n=P}^{N-1}\boldsymbol{x}_l(n)\boldsymbol{x}_l^{\text{H}}(n) + \sum_{k=L}^{L(K+1)-1}\sum_{n=P}^{N-1}\boldsymbol{x}_k(n)\boldsymbol{x}_k^{\text{H}}(n) \quad (37)$$

$$\hat{\boldsymbol{R}}_{yy,l} = \sum_{n=P}^{N-1}\boldsymbol{y}_l(n)\boldsymbol{y}_l^{\text{H}}(n) + \sum_{k=L}^{L(K+1)-1}\sum_{n=P}^{N-1}\boldsymbol{y}_k(n)\boldsymbol{y}_k^{\text{H}}(n) \quad (38)$$

$$\hat{\boldsymbol{R}}_{yx,l} = \sum_{n=P}^{N-1}\boldsymbol{y}_l(n)\boldsymbol{x}_l^{\text{H}}(n) + \sum_{k=L}^{L(K+1)-1}\sum_{n=P}^{N-1}\boldsymbol{y}_k(n)\boldsymbol{x}_k^{\text{H}}(n) \quad (39)$$

and $\hat{\tilde{\boldsymbol{s}}}_{\text{LML}}(n)$ and $\hat{\tilde{\boldsymbol{x}}}_{\text{LML},l}(n)$ are the temporally whitened steering vector and the lth test signal by using the above local ML estimates $\hat{\boldsymbol{A}}_{\text{LML}}$ and $\hat{\boldsymbol{Q}}_{\text{LML}}$.

It is seen that the local ML estimates of $\boldsymbol{A}$ and $\boldsymbol{Q}$ involve 'only' the lth test signal $\boldsymbol{x}_l$ and all training signals. In contrast, the 'global' ML estimates of the GP-Rao test (33) use 'all' L test signals $\{\boldsymbol{x}_l\}_{l=0}^{L-1}$ and all training signals; see (19) and (20) with (13), (14) and (15). In summary, the GP-Rao test can be considered as a non-coherent integration using the local parametric Rao test with the local ML estimates of $\boldsymbol{A}$ and $\boldsymbol{Q}$ replaced by the global ML estimates derived in (19) and (20) in this paper.

3.4 Detection performance

In this section, we analyse the asymptotic distribution of the proposed GP-Rao test. It is known that the Rao test shares the same asymptotic distribution of the GLRT. Following [34], we obtain that

$$T_{\text{GP-Rao}} \overset{\mathcal{A}}{\sim} \begin{cases} \chi_{2L}^2, & \text{under } H_0 \\ \chi_{2L}^2(\rho), & \text{under } H_1 \end{cases} \quad (40)$$

where χ_{2L}^2 denotes the central Chi-squared distribution with $2L$ degrees-of-freedom and $\chi_{2L}^2(\rho)$ the non-central Chi-squared distribution with $2L$ degrees-of-freedom and a non-centrality parameter ρ

$$\rho = 2\sum_{n=P}^{N-1}\tilde{\boldsymbol{s}}^{\text{H}}(n)\boldsymbol{Q}^{-1}\tilde{\boldsymbol{s}}(n)\sum_{l=0}^{L-1}|\alpha_l|^2 \quad (41)$$

where $\tilde{\boldsymbol{s}}$ is the temporally whitened steering vector by using the 'true' AR coefficient matrix $\boldsymbol{A}$; see (8).

Based on the asymptotic distribution of (40), the probability of false alarm is readily shown to be

$$P_{\text{f}} = \mathcal{Q}_{\chi_{2L}^2}(\lambda) \quad (42)$$

where $\mathcal{Q}_{\chi_{2L}^2}(\cdot)$ is the right tail of the central Chi-square χ_{2L}^2 pdf. As a result, the threshold λ can be computed as $\lambda = \mathcal{Q}_{\chi_{2L}^2}^{-1}(P_{\text{f}})$. The result of (42) also shows that the statistical characteristic of the GP-Rao test under H_0 is independent of the nuisance parameters, including the AR coefficient matrix $\boldsymbol{A}$ and the spatial covariance matrix $\boldsymbol{Q}$, and further implies that the GP-Rao test achieves a CFAR property. Meanwhile, the probability of detection can be computed as

$$P_{\text{d}} = \mathcal{Q}_{\chi_{2L}^2(\rho)}(\lambda) \quad (43)$$

where $\mathcal{Q}_{\chi_{2L}^2(\rho)}(\cdot)$ is the right tail of the non-central Chi-square $\chi_{2L}^2(\rho)$ pdf with ρ given by (41).

3.5 Comparison to the covariance matrix-based detectors

In this subsection, the proposed GP-Rao test is compared with the covariance matrix-based detectors including the GLRT [5], the GAMF [5], and the non-parametric Rao and Wald

doi: 10.1049/iet-spr.2011.0313

tests [8] for the range-spread target detection. Notably, these covariance matrix-based detectors all rely on the sample covariance matrix $\hat{\boldsymbol{S}}$ from training signals

$$\hat{\boldsymbol{S}} = \sum_{k=L}^{(K+1)L-1} \boldsymbol{x}_k \boldsymbol{x}_k^{\mathrm{H}} \tag{44}$$

Particularly, the GLRT was developed in [5, eq. (12)] by considering the test and training signal as a whole (i.e. the so-called 'one-step' GLRT strategy [5]) and uses the following test statistic

$$T_{\mathrm{GLRT}} = \frac{\det(\boldsymbol{R}_0 + \hat{\boldsymbol{S}})}{\det(\boldsymbol{R}_1 + \hat{\boldsymbol{S}})} \tag{45}$$

where $|\cdot|$ stands for the matrix determinant, and the matrices $\boldsymbol{R}_0$ and $\boldsymbol{R}_1$ are given by, respectively

$$\boldsymbol{R}_0 = \sum_{l=0}^{L-1} \boldsymbol{x}_l \boldsymbol{x}_l^{\mathrm{H}}$$

$$\boldsymbol{R}_1 = \sum_{l=0}^{L-1} \left(\boldsymbol{x}_l - \frac{\boldsymbol{s}^{\mathrm{H}} \hat{\boldsymbol{S}}^{-1} \boldsymbol{x}_l}{\boldsymbol{s}^{\mathrm{H}} \hat{\boldsymbol{S}}^{-1} \boldsymbol{s}} \boldsymbol{s} \right) \left(\boldsymbol{x}_l - \frac{\boldsymbol{s}^{\mathrm{H}} \hat{\boldsymbol{S}}^{-1} \boldsymbol{x}_l}{\boldsymbol{s}^{\mathrm{H}} \hat{\boldsymbol{S}}^{-1} \boldsymbol{s}} \boldsymbol{s} \right)^{\mathrm{H}}$$

The GAMF, on the other hand, was developed in [5, eq. (25)] by treating the test and training signal as two separate datasets, that is, the 'two-step' GLRT strategy, and uses the following test statistic

$$T_{\mathrm{GAMF}} = \sum_{l=0}^{L-1} \frac{|\boldsymbol{s}^{\mathrm{H}} \hat{\boldsymbol{S}}^{-1} \boldsymbol{x}_l|^2}{\boldsymbol{s}^{\mathrm{H}} \hat{\boldsymbol{S}}^{-1} \boldsymbol{s}} \tag{46}$$

It is seen that the GAMF can be considered as the non-coherent integration of the conventional AMF for the point-target detection [36].

In addition, the 'non-parametric' Rao and Wald detectors were developed in [8] for the compound-Gaussian noise scenario by following the general principle of the Rao and Wald tests. In the homogeneous scenario, the non-parametric Rao and Wald detectors reduce to the following test statistics

$$T_{\mathrm{Rao}} = \sum_{l=0}^{L-1} \frac{|\boldsymbol{s}^{\mathrm{H}} \hat{\boldsymbol{S}}^{-1} \boldsymbol{x}_l|^2}{\boldsymbol{s}^{\mathrm{H}} \hat{\boldsymbol{S}}^{-1} \boldsymbol{s} \sum_{\ell=0}^{L-1} \boldsymbol{x}_\ell^{\mathrm{H}} \hat{\boldsymbol{S}}^{-1} \boldsymbol{x}_\ell} \tag{47}$$

which is a normalised version of the GAMF of (46), and

$$T_{\mathrm{Wald}} = \sum_{l=0}^{L-1} \frac{|\boldsymbol{s}^{\mathrm{H}} \hat{\boldsymbol{S}}^{-1} \boldsymbol{x}_l|^2}{\boldsymbol{s}^{\mathrm{H}} \hat{\boldsymbol{S}}^{-1} \boldsymbol{s} \sum_{\ell=0}^{L-1} (\boldsymbol{x}_\ell^{\mathrm{H}} \hat{\boldsymbol{S}}^{-1} \boldsymbol{x}_\ell - ((|\boldsymbol{s}^{\mathrm{H}} \hat{\boldsymbol{S}}^{-1} \boldsymbol{x}_\ell|^2)/\boldsymbol{s}^{\mathrm{H}} \hat{\boldsymbol{S}}^{-1} \boldsymbol{s}))} \tag{48}$$

which can also be considered as a normalised version of the GAMF. The difference between the non-parametric Rao and Wald tests is the additional normalisation term in the denominator. That is, the non-parametric Rao test computes the normalisation term from the adaptively whitened test signals, whereas the Wald test uses the components of the test signal that are orthogonal to the signal subspace for computation of the normalisation term.

The use of sample covariance matrix usually requires a demanding number of training signals and gives rise to high computational complexity to invert it, especially when the joint space–time dimension JN is large, for example, JN is in the order of hundreds or even thousands. The proposed GP-Rao test, on the other hand, exploits the structured multi-channel AR process of the disturbance and decomposes the jointly spatial–temporal whitening of the covariance matrix-based detector into a successive temporal and spatial whitening, which involves only the inverse of a $J \times J$ matrix. The structured AR process also helps us to mitigate the requirement of excessive training signals. As verified in Section 4, the proposed GP-Rao test works well when the number of training signals KL is significantly less than the joint space–time dimension JN.

4 Numerical examples

In this section, simulation results are provided to verify the analytical result in Section 3.4. Meanwhile, the proposed GP-Rao test is numerically compared with the covariance matrix-based detectors in Section 3.5 including the GLRT (45), the GAMF (46), the non-parametric Rao detector (47), and the Wald detector (48). The disturbance is generated as a multi-channel AR(2) process with AR coefficient $\boldsymbol{A}$ and a spatial covariance matrix $\boldsymbol{Q}$. These parameters are set to ensure that the AR process is stable and that $\boldsymbol{Q}$ is a valid covariance matrix, but otherwise are randomly selected. The signal vector $\boldsymbol{s}$ corresponds to a uniform equispaced linear array with $J = 4$ antenna elements, N temporal pulses, and randomly selected normalised spatial frequency ω_{s} and Doppler frequency ω_{d}, that is

$$\boldsymbol{s} = \boldsymbol{s}_{\mathrm{t}}(\omega_{\mathrm{d}}) \otimes \boldsymbol{s}_{\mathrm{s}}(\omega_{\mathrm{s}}) \tag{49}$$

where $\boldsymbol{s}_t(\omega_d)$ denotes the $N \times 1$ temporal steering vector

$$\boldsymbol{s}_{\mathrm{t}}(\omega_{\mathrm{d}}) = \frac{1}{\sqrt{N}} [1, \mathrm{e}^{\mathrm{j}\omega_{\mathrm{d}}}, \ldots, \mathrm{e}^{\mathrm{j}(N-1)\omega_{\mathrm{d}}}]^{\mathrm{T}} \tag{50}$$

and $\boldsymbol{s}_{\mathrm{s}}(\omega_{\mathrm{s}})$ denotes the $J \times 1$ spatial steering vector

$$\boldsymbol{s}_{\mathrm{s}}(\omega_{\mathrm{s}}) = \frac{1}{\sqrt{J}} [1, \mathrm{e}^{\mathrm{j}\omega_{\mathrm{s}}}, \ldots, \mathrm{e}^{\mathrm{j}(J-1)\omega_{\mathrm{s}}}]^{\mathrm{T}} \tag{51}$$

The signal-to-interference-plus-noise ratio (SINR) is defined as

$$\mathrm{SINR} = \frac{\sum_{l=0}^{L-1} |\alpha_l|^2}{L} \boldsymbol{s}^{\mathrm{H}} \boldsymbol{R}^{-1} \boldsymbol{s} \tag{52}$$

where the $JN \times JN$ covariance matrix $\boldsymbol{R}$ can be uniquely determined once $\boldsymbol{A}$ and $\boldsymbol{Q}$ are selected.

4.1 Limited-training case

We first consider the limited-training cases which are particularly challenging in practice. Specifically, we consider $J = 4$ sensors and $N = 16$ pulses. For the proposed GP-Rao test, we set $K = 4$ and, as a result, there are $KL = 4L = 16$ training signals. In contrast, the covariance matrix-based detectors including the GAMF, the GLRT, the non-parametric Rao and Wald detectors use $K = 96$ and overall $KL = 96L = 384$ training signals. Fig. 1 shows the receiver operating characteristic (ROC) of the GP-Rao test and the covariance matrix-based detectors for

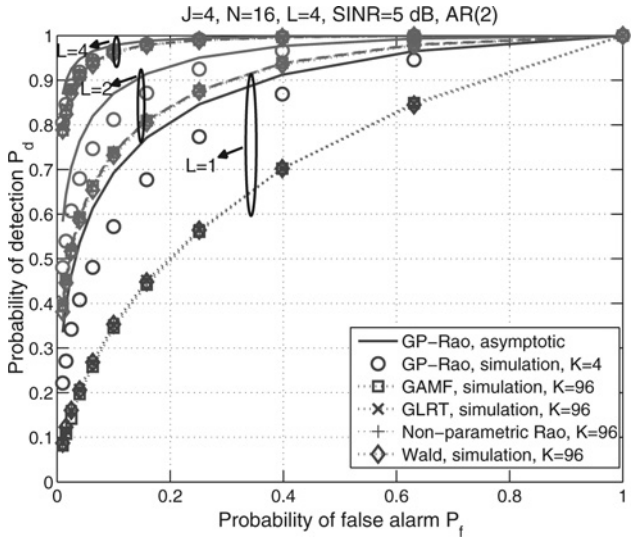

Fig. 1 *ROC curves of the GP-Rao test with $K = 4$ (circle) and the covariance matrix-based detectors with $K = 96$ including the GAMF (square), the GLRT (cross), the non-parametric Rao detector (plus) and the Wald detector (diamond) for various values of L when $J = 4$, $N = 16$, $P = 2$ and SINR = 5 dB*

Asymptotic performance of the GP-Rao test is plotted as the solid curve

various numbers of target scatterers L when SINR = 5 dB. For different cases of L, the target amplitudes are normalised to attain the same SINR. Also included in the figure is the asymptotic detection performance of the GP-Rao test derived in Section 3.4. It is seen that by exploiting the inherent structure of the disturbance covariance matrix, the proposed GP-Rao test with $K = 4$ outperforms the covariance matrix-based detectors with $K = 96$, especially for $L = 1$ and 2. With $KL = 384$ training signals, about six times as large as the overall spatio-temporal dimension $JN = 64$, the performance of the four considered covariance matrix-based detectors converges together. It is easy to conclude that, with overall $KL = 16$ training signals, the GP-Rao test significantly improves the training efficiency of the covariance matrix-based detectors. The asymptotic detection performance of the GP-Rao test provides an upper bound of the simulated results. Moreover, given the same SINR, the more the target scatterers (the larger L is), the better the detection performance. In other words, effectively increasing the radar resolution and suitably exploiting them can produce a potential detection performance gain [4, 5].

Fig. 2 shows the detection probability as a function of SINR in the case of two target scatterers $L = 2$ when the probability of false alarm is fixed at $P_f = 0.01$. The result confirms that the proposed GP-Rao test has better training efficiency – in terms of the number of training signals required to achieve a certain detection probability – than the covariance matrix-based detectors. Particularly, the performance gain achieved is about 0.5 dB for a detection probability at $P_d = 0.9$. Again, with sufficient training signals, the GAMF, the GLRT, the non-parametric Rao and Wald detectors show converged performance, which has about 1.65 dB performance loss to the asymptotic performance of the GP-Rao test at $P_d = 0.6$. In this limited-training scenario with $N = 16$ and $K = 4$, the simulated performance of the GP-Rao test is about 1 dB away from its asymptotic performance at $P_d = 0.6$.

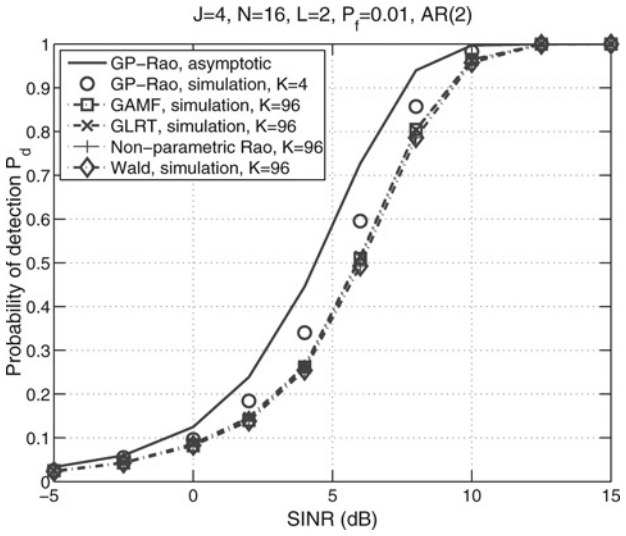

Fig. 2 *Probability of detection as a function of SINR in the limited-training case with $L = 2$ target scatters when $J = 4$, $N = 16$, $P = 2$ and $P_f = 0.01$*

4.2 Large-training case

Next, we increase the value of K for both the parametric GP-Rao test ($K = 32$) and the covariance matrix-based detectors ($K = 128$). This scenario is considered to be a large-training case since the number of training signals is now $KL = 128$ for the GP-Rao test and $KL = 512$ for the covariance matrix-based detectors, which are at least twice larger than the overall space–time dimension $JN = 64$. As shown in Figs. 3 and 4, the GP-Rao test with $K = 32$ is able to achieve the asymptotic performance and provides improved performance over the covariance matrix-based detectors with $K = 128$. Note from Fig. 4 that the performance gain is about 1 dB for a detection probability at $P_d = 0.9$.

4.3 Asymptotic case

An asymptotic scenario with a large value of N (the number of temporal samples) is simulated to verify the asymptotic

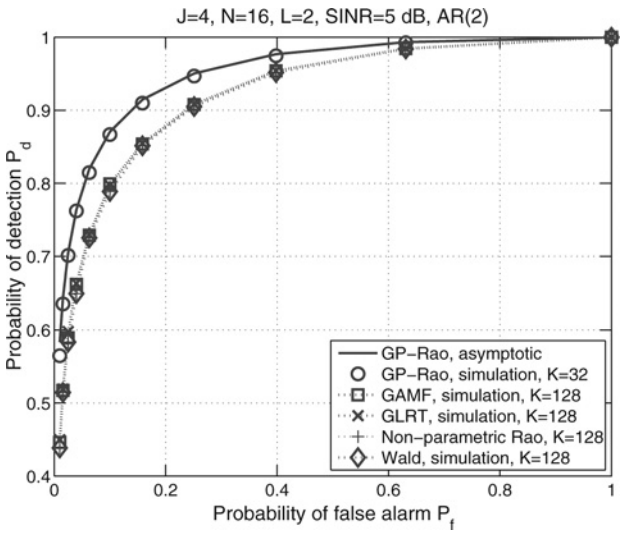

Fig. 3 *ROC of the GP-Rao test with $K = 32$, the GAMF detector with $K = 128$, and the GLRT with $K = 128$ in the case of $L = 2$ target scatters when $J = 4$, $N = 16$, $P = 2$ and SINR = 5 dB*

doi: 10.1049/iet-spr.2011.0313

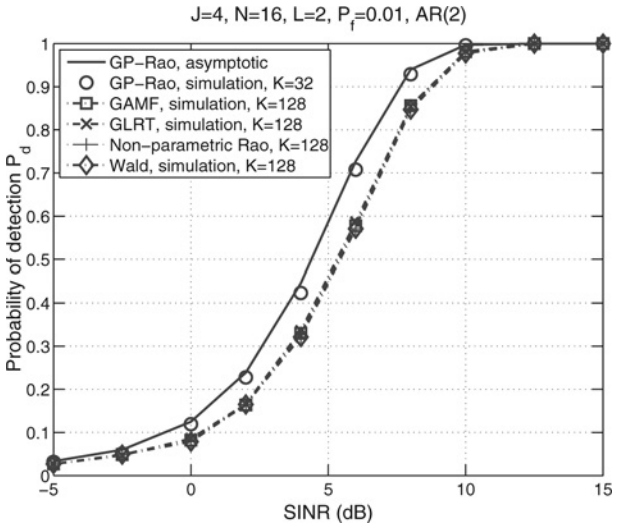

Fig. 4 *Probability of detection as a function of SINR in the large-training case with $L = 2$ target scatters when $J = 4$, $N = 16$, $P = 2$ and $P_f = 0.01$.*

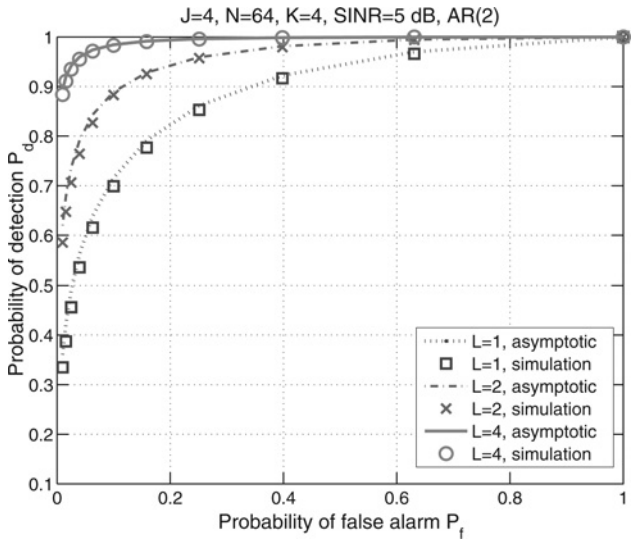

Fig. 5 *Asymptotic performance ($N = 64$) of the GP-Rao test in the limited-training ($K = 4$) case for various values of L when $J = 4$, $P = 2$ and SINR = 5 dB*

performance of the GP-Rao test derived in Section 3.4. Whereas keeping the other system parameters (J, K, P and SINR) the same as the ones in Fig. 1, we consider $N = 64$, which is comparatively much larger than the number of sensors ($J = 4$). The result is shown in Fig. 5 for three cases of L. It is seen that, even if the training signals are limited ($K = 4$), increasing the number of temporal sampling (or, equivalently, the number of pulses), the probability of detection can still approach the asymptotic performance of the GP-Rao test. This observation has been made for a point-target ($L = 1$) case [26] and here extended for the range-spread target ($L = 2$ and 4) case as shown in Fig. 5. This is equivalent to saying that the performance loss of the GP-Rao test due to limited-training sises can be compensated for by utilising longer temporal observation interval, that is, N is large.

5 Conclusion

In this paper, the problem of adaptive detection of a range-spread target in a homogeneous environment was considered. The disturbances in both the test signals and training signals were modelled as a multi-channel AR process, which enables a parametric detector for the range-spread target detection. We adopted the Rao test and developed the GP-Rao test for the range-spread target detection case. The GP-Rao test was shown to be a non-coherent integration of the local parametric Rao test by replacing the local ML estimates by the globe ML estimates of unknown parameters. The detection performance was also characterised by the asymptotic distribution of the GP-Rao test under both hypotheses. The analytical result revealed that the GP-Rao test was a CFAR detector in an asymptotic sense. Numerical results verified that the GP-Rao test achieved improved performance over that of covariance matrix-based detectors including the GAMF, the GLRT, the non-parametric Rao and Wald tests, especially in the case of training-limited scenarios.

6 Acknowledgment

The authors would like to thank the anonymous reviewers for their valuable comments and suggestions. This work was supported, through a sub-contract to Dynetics, by the Air Force Research Laboratory, RF Technology Branch (AFRL/RYMD) under Contract FA8650-08-D-1303.

7 References

1 Hughes, P.K.: 'A high-resolution Radar detection strategy', *IEEE Trans. Aerosp. Electron. Syst.*, 1983, **19**, (5), pp. 663–667
2 Wehner, D.R.: 'High-resolution radar' (Artech House, Norwell, MA, 1995, 2nd edn.)
3 Gerlach, K., Steiner, M.J., Lin, F.C.: 'Detection of a spatially distributed target in white noise', *IEEE Signal Process. Lett.*, 1997, **4**, (7), pp. 198–200
4 Gerlach, K., Steiner, M.J., Lin, F.C.: 'Adaptive detection of range distributed targets', *IEEE Trans. Signal Process.*, 1999, **47**, (7), pp. 1844–1851
5 Conte, E., De Maio, A., Ricci, G.: 'GLRT-based adaptive detection algorithms for range-spread targets', *IEEE Trans. Signal Process.*, 2001, **49**, (7), pp. 1336–1348
6 Gerlach, K.: 'Spatially distributed target detection in non-Gaussian clutter', *IEEE Trans. Aerosp. Electron. Syst.*, 1999, **35**, (3), pp. 926–934
7 Conte, E., De Maio, A., Ricci, G.: 'CFAR detection of distributed targets in non-Gaussian disturbance', *IEEE Trans. Aerosp. Electron. Syst.*, 2002, **38**, (2), pp. 612–621
8 Conte, E., De Maio, A.: 'Distributed target detection in compound-Gaussian noise with Rao and Wald tests', *IEEE Trans. Aerosp. Electron. Syst.*, 2003, **39**, (2), pp. 568–582
9 Alfano, G., De Maio, A., Farina, A.: 'Model-based adaptive detection of range-spread targets', *IEE Proc.: Radar, Sonar Navig.*, 2004, **151**, (1), pp. 2–10
10 Bandiera, F., Ricci, G.: 'Adaptive detection and interference rejection of multiple point-like radar targets', *IEEE Trans. Signal Process.*, 2006, **54**, (12), pp. 4510–4518
11 De Maio, A., Farina, A., Gerlach, K.: 'Adaptive detection of range spread targets with orthogonal rejection', *IEEE Trans. Aerosp. Electron. Syst.*, 2007, **43**, (2), pp. 738–752
12 Bandiera, F., De Maio, A., Ricci, G.: 'Adaptive radar detection of distributed targets in homogeneous and partially homogeneous noise plus subspace interference', *IEEE Trans. Signal Process.*, 2007, **55**, (4), pp. 1223–1237
13 Bon, N., Khenchaf, A., Garello, R.: 'GLRT subspace detection for range and doppler distributed targets', *IEEE Trans. Aerosp. Electron. Syst.*, 2008, **44**, (2), pp. 678–695
14 Bandiera, F., Orlando, D., Ricci, G.: 'CFAR detection strategies for distributed targets under conic constraints', *IEEE Trans. Signal Process.*, 2009, **57**, (9), pp. 3305–3316

15 He, Y., Jian, T., Su, F., Qu, C., Gu, X.: 'Novel range-spread target detectors in non-Gaussian clutter', *IEEE Trans. Aerosp. Electron. Syst.*, 2010, **46**, (3), pp. 1312–1328
16 Guan, J., Zhang, X.: 'Subspace detection for range and doppler distributed targets with Rao and Wald tests', *Signal Process.*, 2011, **91**, (1), pp. 51–60
17 Shui, P.-L., Xu, S.-W., Liu, H.-W.: 'Range-spread target detection using consecutive HRRPs', *IEEE Trans. Aerosp. Electron. Syst.*, 2011, **47**, (1), pp. 647–665
18 Bandiera, F., Besson, O., Ricci, G.: 'Adaptive detection of distributed targets in compound-Gaussian noise without secondary data: a Bayesian approach', *IEEE Trans. Signal Process.*, 2011, **59**, (12), pp. 5698–5708
19 Jian, T., He, Y., Su, F., Qu, C., Ping, D.: 'Adaptive detection of sparsely distributed target in non-Gaussian clutter', *IET Radar, Sonar Navig.*, 2011, **5**, (7), pp. 780–787
20 Jian, T., He, Y., Su, F., Qu, C.: 'Adaptive range-spread target detection based on modified generalised likelihood ratio test in non-Gaussian clutter', *IET Radar, Sonar Navig.*, 2011, **5**, (9), pp. 970–977
21 Ward, J.: 'Space-time adaptive processing for airborne radar'. Technical Report 1015, Lincoln Laboratory, MIT, December 1994
22 Klemm, R.: 'Principles of space-time adaptive processing' (The Institute of Electrical Engineers, London, UK, 2002)
23 Romäan, J.R., Rangaswamy, M., Davis, D.W., Zhang, Q., Himed, B., Michels, J.H.: 'Parametric adaptive matched filter for airborne radar applications', *IEEE Trans. Aerosp. Electron. Syst.*, 2000, **36**, (2), pp. 677–692
24 Parker, P., Swindlehurst, A.L.: 'Space-time auto-regressive filtering for matched subspace STAP', *IEEE Trans. Aerosp. Electron. Syst.*, 2003, **39**, (2), pp. 510–520
25 Lawrence Marple, S. Jr., Corbell, P.M., Rangaswamy, M.: 'Multichannel fast parametric algorithms and performance for adaptive radar'. Proc. 41st Asilomar Conf. on Signals, Systems, and Computers, Pacific Grove, CA, November 2007, pp. 1835–1838
26 Sohn, K.J., Li, H., Himed, B.: 'Parametric Rao test for multichannel adaptive signal detection', *IEEE Trans. Aerosp. Electron. Syst.*, 2007, **43**, (3), pp. 920–933
27 Sohn, K.J., Li, H., Himed, B.: 'Parametric GLRT for multichannel adaptive signal detection', *IEEE Trans. Signal Process.*, 2007, **55**, (11), pp. 5351–5360
28 Abramovich, Y.I., Spencer, N.K., Turley, M.D.E.: 'Time-varying autoregressive (TVAR) models for multiple radar observations', *IEEE Trans. Signal Process.*, 2007, **55**, (4), pp. 1298–1311
29 Lawrence Marple, S. Jr., Corbell, P.M., Rangaswamy, M.: 'Performance tradeoffs for multi-channel parametric adaptive radar algorithms'. Proc. 2008 Int. Conf. on Radar, September 2008, pp. 154–159
30 Wang, P., Li, H., Himed, B.: 'A new parametric GLRT for multichannel adaptive signal detection', *IEEE Trans. Signal Process.*, 2010, **58**, (1), pp. 317–325
31 Wang, P., Li, H., Himed, B.: 'A Bayesian parametric test for multichannel adaptive signal detection in non-homogeneous environments', *IEEE Signal Process. Lett.*, 2010, **17**, (4), pp. 351–354
32 Wang, P., Li, H., Himed, B.: 'Parametric Rao tests for multichannel adaptive detection in partially homogeneous environment', *IEEE Trans. Aerosp. Electron. Syst.*, 2011, **47**, (3), pp. 1850–1862
33 Wang, P., Li, H., Himed, B.: 'Knowledge-aided parametric tests for multichannel adaptive signal detection', *IEEE Trans. Signal Process.*, 2011, **59**, (12), pp. 5970–5982
34 Kay, S.M.: 'Fundamentals of statistical signal processing: detection theory' (Prentice Hall, Upper Saddle River, NJ, 1998)
35 De Maio, A.: 'Rao test for adaptive detection in Gaussian interference with unknown covariance matrix', *IEEE Trans. Signal Process.*, 2007, **55**, (7), pp. 3577–3584
36 Robey, F.C., Fuhrmann, D.R., Kelly, E.J., Nitzberg, R.: 'A CFAR adaptive matched filter detector', *IEEE Trans. Aerosp. Electron. Syst.*, 1992, **28**, (1), pp. 208–216

doi: 10.1049/iet-spr.2011.0313